Journal Pre-proof

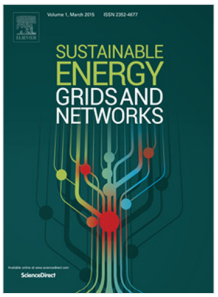

Hydraulic transient modeling and analysis of the district heating network

Xuejing Zheng, Boxiao Xu, Yaran Wang, Shijun You, Huan Zhang,
Shen Wei, Na Wang

PII: S2352-4677(20)30340-4
DOI: https://doi.org/10.1016/j.segan.2020.100409
Reference: SEGAN 100409

To appear in: *Sustainable Energy, Grids and Networks*

Received date : 19 June 2020
Revised date : 30 September 2020
Accepted date : 9 November 2020

Please cite this article as: X. Zheng, B. Xu, Y. Wang et al., Hydraulic transient modeling and analysis of the district heating network, *Sustainable Energy, Grids and Networks* (2020), doi: https://doi.org/10.1016/j.segan.2020.100409.

Hydraulic transient modeling and analysis of the district heating network

Xuejing Zheng [a, b], Boxiao Xu [a], Yaran Wang [a, b, *], Shijun You [a, b], Huan Zhang [a, b], Shen Wei [c], Na Wang [d]

[a] School of Environmental Science and Engineering, Tianjin University, Tianjin 300350, PR China

[b] Tianjin Key Lab of Biomass/Wastes Utilization, Tianjin 300350, PR China

[c] The Bartlett School of Construction and Project Management, University College London (UCL), 1-19 Torrington Place, London WC1E 7HB, United Kingdom

[d] Tianjin Energy Investment Group CO. LTD., Tianjin 300072, PR China

[*] Corresponding author.

Tel. / Fax: +86 22 2740 0832.

E-Mail address: yaran_wang@tju.edu.cn.

Abstract

The hydraulic transients are obvious during the operation and adjustment of large-scale district heating (DH) network. Hydraulic transient modeling and simulation methods can provide basis for efficient operation of the DH network. In this paper, two hydraulic transient models, the distributed parameter model (DPM) and lumped parameter model (LPM), were established for DH network. Efficient numerical algorithms were presented for the two models. The proposed DPM and LPM were both applied to a DH network to simulate and analyze the network hydraulic transients caused by the valve and pump operations. Results indicate that with the increase of the distance from the adjustment location, the transient time for the flow rate and pressure gets longer. As the adjustment duration decreases, the

transient time increases. Comparison of the simulation performances between the two models indicates that the DPM can capture the high-frequency hydraulic transients subtly. With the decrease of adjustment duration, more severe high-frequency hydraulic transients will occur. However, only the average hydraulic fluctuations can be described by LPM. The computation time of LPM is shorter than DPM because of the vectorizable calculation procedure and the less data to record, since the LPM neglects the pressure waves and the fluid compressibility.

Keywords: district heating network; hydraulic transient; distributed parameter model; lumped parameter model; transient time .

Nomenclature			
a	Pressure wave velocity (m/s)	Q_t	Flow rate vector of tree branches (m^3/h)
α	Dimensionless frequency ratio of the pump	R_v	Adjustable ratio of valve
A	Cross-sectional area of pipeline (m^2)	S	Impedance of heat exchanger [$m/(m^3/h)^2$]
B_k	Basic incidence matrix of district heating network	S^*	Comprehensive impedance of pipeline [$m/(m^3/h)^2$]
B_{kr}	Incidence matrix of cotree branches	t	Time (s)
B_{kt}	Incidence matrix of tree branches	T	Real-world calculation time (s)
c_1, c_2, c_3	Parameters of pump characteristic equation	Δt	Time steps (s)
C_f	Independent loop matrix of district heating network	ω	Valve opening
C_{v0}	Flow capacity for $\omega = 100\%$	x	Axial length of the pipeline (m)
D	Diameter of pipeline (m)	Δx	Spatial steps (m)
f	Resistance coefficient	ϕ	Resistance of valve at heat exchanger [$m/(m^3/h)^2$]
F	Operating frequency (Hz)	ρ	Hot water density (kg/m^3)
F_0	Rated frequency (Hz)	*Subscripts*	
g	Acceleration of gravity (m/s^2)	i	Number of nodes on the pipeline
H	Pressure head (m)	j	Pipeline number
H_c	Pressure at pipeline junction (m)	j_r	Number of supply pipeline
H_p	Pump head vector of all circulating pumps (m)	j_s	Number of return pipeline
H_0	Constant pressure of circulating pump inlet at the referenced heat source (m)	k	Number of nodes used in calculation of each pipeline connected at the junction
ΔH	Resistance loss of pipeline (m)	*Superscripts*	
ΔH^*	Pressure drop vector between inlets and outlets of all the pipelines (m)	n	Last time step
I_r	Identity matrix	$n+1$	Present time step
L	Length of pipeline (m)	*Abbreviations*	
N	Quantity of control volumes	DH	District heating
NS	Last node at downstream of pipeline	DPM	Distributed parameter model
Q	Flow rate (m^3/h)	LPM	Lumped parameter model
Q_b	Flow rate of make-up water (m^3/h)	ODE	Ordinary differential equation
Q_h	Flow rate of heat exchanger pipeline (m^3/h)	PDE	Partial differential equation
Q_s	Flow rate of heat source pipeline (m^3/h)	4GDH	4th generation district heating
Q_r	Flow rate vector of cotree branches (m^3/h)		

1. Introduction

The district heating (DH) system is one of the most essential infrastructures in modernized city, which is of great significance for energy saving and emission reduction. Combined with smart energy systems, waste heat and renewable energy sources can be integrated into DH system to achieve high energy efficiency, as the 4th generation district heating (4GDH) is introduced in [1]. With the development of 4GDH, the DH networks need higher operational flexibility, which depends on the advancements of modeling and simulation technology. The analysis on hydraulic characteristics of DH network is extremely important, because the hydraulic conditions directly affect the efficiency of transmission, distribution and operation of the DH network.

The static hydraulic modeling methods are widely used to analyze the operation and adjustment of DH network. In the static hydraulic model, the flow rates and pressures of the network are correlated by the steady-state Bernoulli equations of all the pipelines and the Kirchhoff's laws. The flow rates and pressures of the DH network can be calculated by iterative methods of non-linear equations [2]. A static hydraulic simulation method of meshed DH network with multiple heat sources was presented based on square roots method, which required less iteration steps and faster computational speed [3]. A hydraulic simulation platform [4] was established based on the static hydraulic model of meshed DH network with two or three heat sources, and the simulation results are also validated by measured data [5,6]. Based on the

static hydraulic model, various control strategies of DH network were proposed [7,8]. An optimal control strategy of DH network was developed by proper orthogonal decomposition with radial basis functions method [9], which can efficiently reduce the energy consumption of the DH system and manage the malfunction conditions.

However, the unsteady variations of the flow rates and pressures within the DH network cannot be ignored during the operation and adjustment of the DH network. Studies on the modeling and simulation of the hydraulic transients will provide technical support for dynamic regulation of large-scale DH network [2]. The hydraulic characteristic of the district heating system was described based on the graph theory and the unsteady flow equation of the pipeline, which showed the relationship between the pressure along the pipeline and the derivative of flow rate with respect to time [10]. A hydraulic transient model of the district heating pipeline was established based on momentum and continuity equation, the similitude criterions used in analysis of the flow of compressible fluid were deduced. The proper pipes for the scale model of the long-distance district heating system were selected by experiments based on several typical parameters of the pipes [11]. In our previous research, a lumped parameter model (LPM) and its numerical solution method for DH network have been proposed, which were effectively applied to simulate and analyze the dynamic responses of the substation flow rates during the unsteady hydraulic processes in real DH networks [2,12]. The LPM assumes uniform flow rate along each pipeline at a certain time, while the pressure wave propagation along the pipeline

and the compressibility of the fluid are neglected. The transient fluid flow of each pipeline is governed by an ordinary differential equation (ODE), the Bernoulli's equation for unsteady flow. Combination of all these ODEs for the pipelines of the whole DH network with Kirchhoff's laws will lead to the LPM [12]. The neglect of pressure wave propagation and compressibility of the fluid will result in imprecision of the network hydraulic transient analysis. The distributed parameter model (DPM), which considers these two factors, is essential for more precise hydraulic transient simulation of the DH network. However, the research on the DPM of DH network hydraulic transient is rare.

The DPM of the water distribution networks, gas transmission networks and petroleum transmission networks for hydraulic transient modeling and simulation have been extensively studied. The DPMs of these networks are established by solving the momentum and continuity equations of all the pipelines considering the Kirchhoff's laws numerically. A DPM and three of its solution methods were constructed and applied to the hydraulic transient analysis of water distribution networks with different size and complexity, the comparable accuracy of DPM was shown [13]. A DPM of gas supply network was established and used in a real gas transportation system, the transient gas flow was simulated precisely in the normal and supply reduction case [14]. Based on the subtle simulation of transient flow in real long-distance main feeder [15] and water distribution network [16] by DPM, the rational designs of the systems can be determined to prevent extremely high pressure

and other security accidents. The accuracy and reliability of the DPM have been verified by experiments in various researches [17-20]. The existing researches indicate that the DPMs can precisely predict the hydraulic transients of fluid networks, hence it is feasible to be applied to the DH network. However, the DH network is a closed fluid network with supply and return pipelines forming all the circulation loops, the previous DPMs for the open networks cannot be directly applied to the DH network. For the further application of the DPM, since the propagation of the pressure wave and high-frequency hydraulic fluctuations can be subtly captured by the DPM, the water hammer protection and the rapid leakage detection of the large-scale district heating networks can be realized based on the hydraulic transient analysis [21,22].

In this paper, the DPM of DH network for hydraulic transient simulation was established. The characteristic line method was introduced to solve the DPM. Boundary conditions including pipeline junctions, heat exchangers and heat sources were developed. By neglecting the pressure wave propagation and the compressibility of the fluid, a simplified LPM can also be derived. The fourth-order Runge-Kutta method was proposed to solve the LPM. The DPM and LPM were both applied to the simulation study of a real DH network. The independence tests of the spatial and time steps were conducted on both numerical models. The hydraulic transient characteristics were analyzed by the DPM and LPM during the adjustments of substation valve opening and heat source circulating pump frequency, the two models were comprehensively compared with each other to study the differences in hydraulic

transient analysis.

2. Methods

2.1. Distributed parameter model

The hydraulic transients of all the DH pipelines and their boundary conditions including junctions of three or more pipelines, heat exchangers and heat sources are considered to establish the unsteady hydraulic model of a whole DH network. The momentum and continuity equations that describe the hydraulic transient characteristics of the pipeline are formulated as [23]:

$$\frac{1}{A}\frac{\partial Q}{\partial t}+g\frac{\partial H}{\partial x}+\frac{f}{2DA^2}Q|Q|=0 \tag{1}$$

$$\frac{\partial H}{\partial t}+\frac{a^2}{gA}\frac{\partial Q}{\partial x}=0 \tag{2}$$

where g (m/s^2) is the acceleration of gravity, H (m) is the pressure head, x (m) is the axial length of the pipeline, Q (m^3/h) is the flow rate, A (m^2) is the cross-sectional area of the pipeline, t (s) is the time, f is the resistance coefficient, D (m) is the diameter of pipeline, a (m/s) is pressure wave velocity. The characteristic line method [23] is used to convert the partial differential equations (PDEs) into ODEs as Eqs. (3) ~ (6). Eqs. (3) and (4) are applicable to positive characteristic line (AP), while Eqs. (5) and (6) are applicable to negative characteristic line (BP), as shown in Fig. 1. The characteristic lines represent the propagation paths of pressure wave.

$$\frac{1}{a}\frac{dH}{dt}+\frac{1}{gA}\frac{dQ}{dt}+\frac{f}{2gDA^2}Q|Q|=0 \tag{3}$$

$$\frac{dx}{dt} = a \tag{4}$$

$$-\frac{1}{a}\frac{dH}{dt} + \frac{1}{gA}\frac{dQ}{dt} + \frac{f}{2gDA^2}Q|Q| = 0 \tag{5}$$

$$\frac{dx}{dt} = -a \tag{6}$$

Eqs. (3) and (5) are discretized as Eqs. (7) and (8) along the positive and negative characteristic line [23]. $C_{j,i\text{-}1}$ and $C_{j,i+1}$ is calculated by Eqs. (9) and (10).

$$H_{j,i}^{n+1} = C_{j,i\text{-}1} - B_j Q_{j,i}^{n+1} \tag{7}$$

$$H_{j,i}^{n+1} = C_{j,i+1} + B_j Q_{j,i}^{n+1} \tag{8}$$

$$C_{j,i\text{-}1} = H_{j,i-1}^{n} + B_j Q_{j,i-1}^{n} - R_j Q_{j,i-1}^{n} \left| Q_{j,i-1}^{n} \right| \tag{9}$$

$$C_{j,i+1} = H_{j,i+1}^{n} - B_j Q_{j,i+1}^{n} + R_j Q_{j,i+1}^{n} \left| Q_{j,i+1}^{n} \right| \tag{10}$$

where i is number of nodes on the pipeline, n is last time step, $n+1$ is present time step, B_j and R_j is calculated by Eq. (11) and (12), respectively.

$$B_j = \frac{a_j}{gA_j} \tag{11}$$

$$R_j = \frac{f_j \Delta x_j}{2gD_j A_j^{\,2}} \tag{12}$$

As shown in Fig. 1, when the flow rates and pressures of two adjacent nodes (A and B) at the previous time step n are known, the flow rate and pressure of the node (P) at the present time step $n+1$ can be calculated by Eq. (7) ~ (9). By analogy, the flow rate and pressure of all internal nodes of the pipeline at each time step can be obtained.

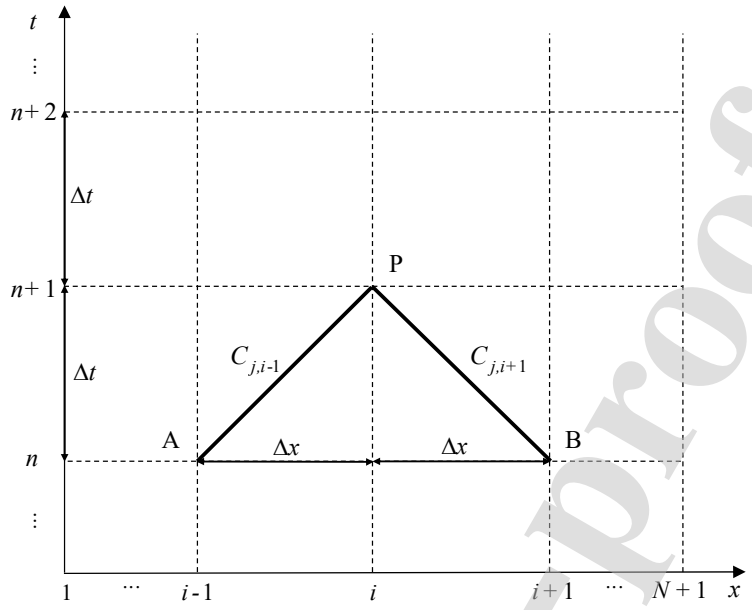

Fig. 1. Characteristic lines of a single pipeline

The flow rate and pressure boundary conditions of boundary nodes of the pipelines, including the pipeline junctions, heat exchangers and heat sources are developed as follows.

(1) *Pipeline junctions*

In DH network, the node connecting three or more pipelines is called the pipeline junction, as shown in Fig. 2. The hydraulic characteristics of the junction are governed by two control equations: 1) the pressure of each pipeline at the junction is equal, as described by Eq. (13); 2) the conservation of mass is satisfied at the junction, which means the net flow rate of inflow and outflow at the junction are the same, as Eq. (14).

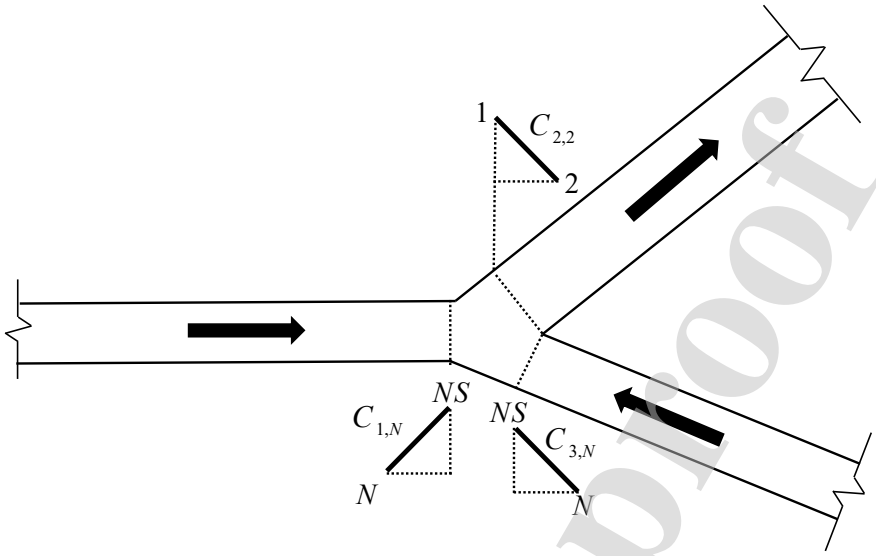

Fig. 2. Hydraulic schematic of pipeline junction

$$H_{1,NS}^{n+1} = H_{2,1}^{n+1} = H_{3,NS}^{n+1} = H_c \tag{13}$$

$$Q_{1,NS}^{n+1} + Q_{3,NS}^{n+1} = Q_{2,1}^{n+1} \tag{14}$$

where N is penultimate node, whose number is equal to the quantity of control volumes, NS is the last node at downstream of the pipeline, H_c (m) is the pressure at the pipeline junction. The characteristic line equations at the junction are shown as Eqs. (15) ~ (17).

$$Q_{1,NS}^{n+1} = \frac{C_{1,N} - H_{1,NS}^{n+1}}{B_1} \tag{15}$$

$$Q_{2,1}^{n+1} = \frac{H_{2,2}^{n+1} - C_{2,2}}{B_2} \tag{16}$$

$$Q_{3,NS}^{n+1} = \frac{C_{3,N} - H_{3,NS}^{n+1}}{B_3} \tag{17}$$

The junction pressure can be obtained by solving Eqs. (9), (10), (13) ~ (17) simultaneously, and formulated as Eq. (18).

$$H_c = \frac{\frac{C_{1,N}}{B_1} + \frac{C_{2,2}}{B_2} + \frac{C_{3,N}}{B_3}}{\frac{1}{B_1} + \frac{1}{B_2} + \frac{1}{B_3}} \tag{18}$$

Since the flow direction does not influence the form of the equations, the pressure at the junction can be converted into the following general form:

$$H_c = \frac{\sum_j \frac{C_{j,k}}{B_j}}{\sum_j \frac{1}{B_j}} \tag{19}$$

where k is the number of nodes used in calculation of each pipeline connected at the junction (node number 2 or N of the pipeline). The flow rate at the junction of each pipeline can be calculated by substituting Eq. (19) into Eqs. (15) ~ (17).

(2) *Heat exchangers*

The heat exchanger in each substation is considered as a resistance component in DPM. There are only two nodes at the inlet and outlet of the heat exchanger, connecting two pipelines j_s and j_r (j_s represents the number of supply pipeline, and j_r represents the number of return pipeline), respectively, as shown in Fig. 3. The flow rates at the end node of j_s and the first node of j_r are equal, and the pressure difference of the inlet and outlet node 1 and node 2 equals the resistance of the heat exchanger and the valve, as Eqs. (20) ~ (23).

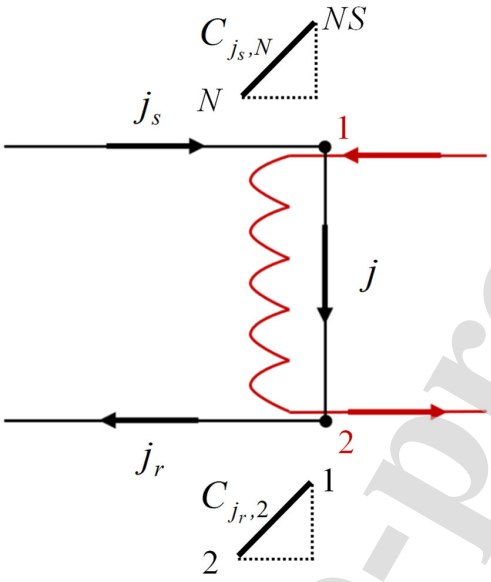

Fig. 3. Hydraulic schematic of heat exchanger

$$Q_{j,1}^{n+1} = Q_{j_s,NS}^{n+1} = Q_{j,2}^{n+1} = Q_{j_r,1}^{n+1} = Q_h \tag{20}$$

$$H_{j,1}^{n+1} = H_{j_s,NS}^{n+1} \tag{21}$$

$$H_{j,2}^{n+1} = H_{j_r,1}^{n+1} \tag{22}$$

$$H_{j,1}^{n+1} - H_{j,2}^{n+1} = H_{j_s,NS}^{n+1} - H_{j_r,1}^{n+1} = (S_j + \phi_j) Q_h^{\,2} \tag{23}$$

where Q_h (m^3/h) is the flow rate of heat exchanger pipeline, S [$m/(m^3/h)^2$] is the impedance of the heat exchanger and its fittings. Combined with Eqs. (7) ~ (10), the flow rate of heat exchanger can be formulated as Eq. (24).

$$Q_h = \frac{-(B_{j_s} + B_{j_r}) \pm \sqrt{(B_{j_s} + B_{j_r})^2 + 4S_j(C_{j_s,N} - C_{j_r,2})}}{2(S_j + \phi_j)} \tag{24}$$

where ϕ [$m/(m^3/h)^2$] is the impedance of valve at heat exchanger, which can be calculated by Eq. (25).

$$\phi_j = \rho \left(\frac{R_v^{(1-\omega_j)}}{C_{v0,j}} \right)^2 \tag{25}$$

The valve at the primary side of the heat exchanger has the equal percentage flow characteristic. ω is the valve opening, C_{v0} is flow capacity for valve opening ω =100%, R_v is rangeability of the valve, ρ (kg/m^3) is the hot water density. Substitute Eq. (24) into Eqs. (7) and (8), the inlet and outlet pressures can be obtained using Eqs. (21) and (22).

(3) *Heat sources*

The heat source of DH network includes a heat exchanger and a circulating pump, as shown in Fig. 4. For the DH network with multiple heat sources, the pump inlet of a certain heat source (named the referenced heat source) is specified as a constant pressure level, maintained by the make-up pump. Mathematical models of the two types of heat sources, the referenced heat source and non-referenced heat sources, are established respectively. The inlet and outlet node of heat source connects pipeline j_r and j_s, respectively, the flow rate and pressure are calculated with Eqs. (26) ~ (29). The inlet and outlet pressure difference of the heat source equals to the difference between the pump head and resistance of the heat source.

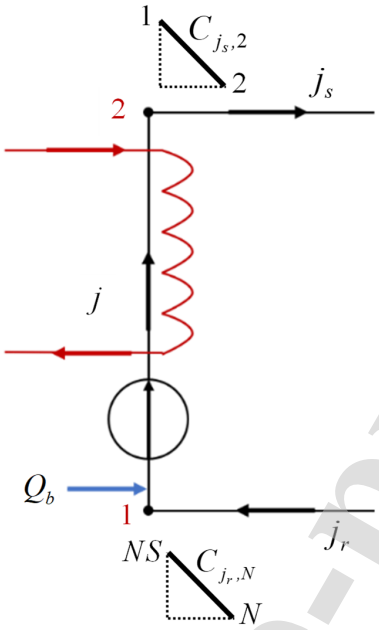

Fig. 4. Hydraulic schematic of heat source

$$Q_{j,1}^{n+1} = Q_{j_r,NS}^{n+1} = Q_{j,2}^{n+1} = Q_{j_s,1}^{n+1} = Q_s \tag{26}$$

$$H_{j,1}^{n+1} = H_{j_r,NS}^{n+1} \tag{27}$$

$$H_{j,2}^{n+1} = H_{j_s,1}^{n+1} \tag{28}$$

$$H_{j,2}^{n+1} - H_{j,1}^{n+1} = H_{j_s,1}^{n+1} - H_{j_r,NS}^{n+1} = c_1 Q_s^{\,2} + c_2 \alpha Q_s + c_3 \alpha^2 - S_j Q_s^2 \tag{29}$$

where Q_s (m^3/h) is the flow rate of heat source , c_1, c_2 and c_3 are parameters of the pump characteristic curve, α is the dimensionless frequency ratio of the pump, which is a function of time:

$$\alpha = \frac{F}{F_0} \tag{30}$$

where F (Hz) is the operating frequency, F_0 (Hz) is the rated frequency. Combined with Eqs. (7) ~ (10), the flow rate of heat source pipeline can be solved as

Eq. (31). The inlet and outlet pressures can be obtained by Eqs. (7) and (8).

$$Q_s = \frac{-(c_2\alpha - B_{j_s} - B_{j_r}) \pm \sqrt{(c_2\alpha - B_{j_s} - B_{j_r})^2 + 4(c_1 - S_j)(c_3\alpha^2 + C_{j_s,2} - C_{j_r,N})}}{2(c_1 - S_j)} \quad (31)$$

For the referenced heat source, the make-up water is installed at the inlet of the circulating pump to ensure that the empty and vaporization do not occur. The flow rate of the make-up water equals to the flow difference between the inlet and outlet of the circulating pump. Mathematical model of the constant pressure replenishment system is governed by Eqs. (32) ~ (35). The inlet flow rate of the circulating pump can be calculated as Eq. (36). The pressure difference between the inlet and outlet of the referenced heat source is formulated as Eq. (37). The outlet flow rate of the referenced heat source is calculated as Eq. (38).

$$Q_{j,1}^{n+1} = Q_{j_r,NS}^{n+1} \quad (32)$$

$$Q_{j,2}^{n+1} = Q_{j_s,1}^{n+1} \quad (33)$$

$$Q_b = Q_{j,2}^{n+1} - Q_{j,1}^{n+1} = Q_{j_s,1}^{n+1} - Q_{j_r,NS}^{n+1} \quad (34)$$

$$H_{j,1}^{n+1} = H_{j_r,NS}^{n+1} = H_0 \quad (35)$$

$$Q_{j,1}^{n+1} = \frac{C_{j_r,N} - H_0}{B_{j_r}} \quad (36)$$

$$H_{j,2}^{n+1} - H_{j,1}^{n+1} = H_{j_s,1}^{n+1} - H_{j_r,NS}^{n+1} = c_1(Q_{j,2}^{n+1})^2 + c_2\alpha Q_{j,2}^{n+1} + c_3\alpha^2 - S_j(Q_{j,2}^{n+1})^2 \quad (37)$$

$$Q_{j,2}^{n+1} = Q_{j_s,1}^{n+1} = \frac{-(c_2\alpha - B_{j_s}) \pm \sqrt{(c_2\alpha - B_{j_s})^2 - 4(c_1 - S_j)(c_3\alpha^2 - C_{j_s,2} + H_0)}}{2(c_1 - S_j)} \quad (38)$$

where H_0 (m) is the maintained constant pressure of the circulating pump inlet at the referenced heat source, Q_b (m^3/h) is the flow rate of the make-up water. The detailed hydraulic transient calculation procedures of the DPM are shown in Fig. 5.

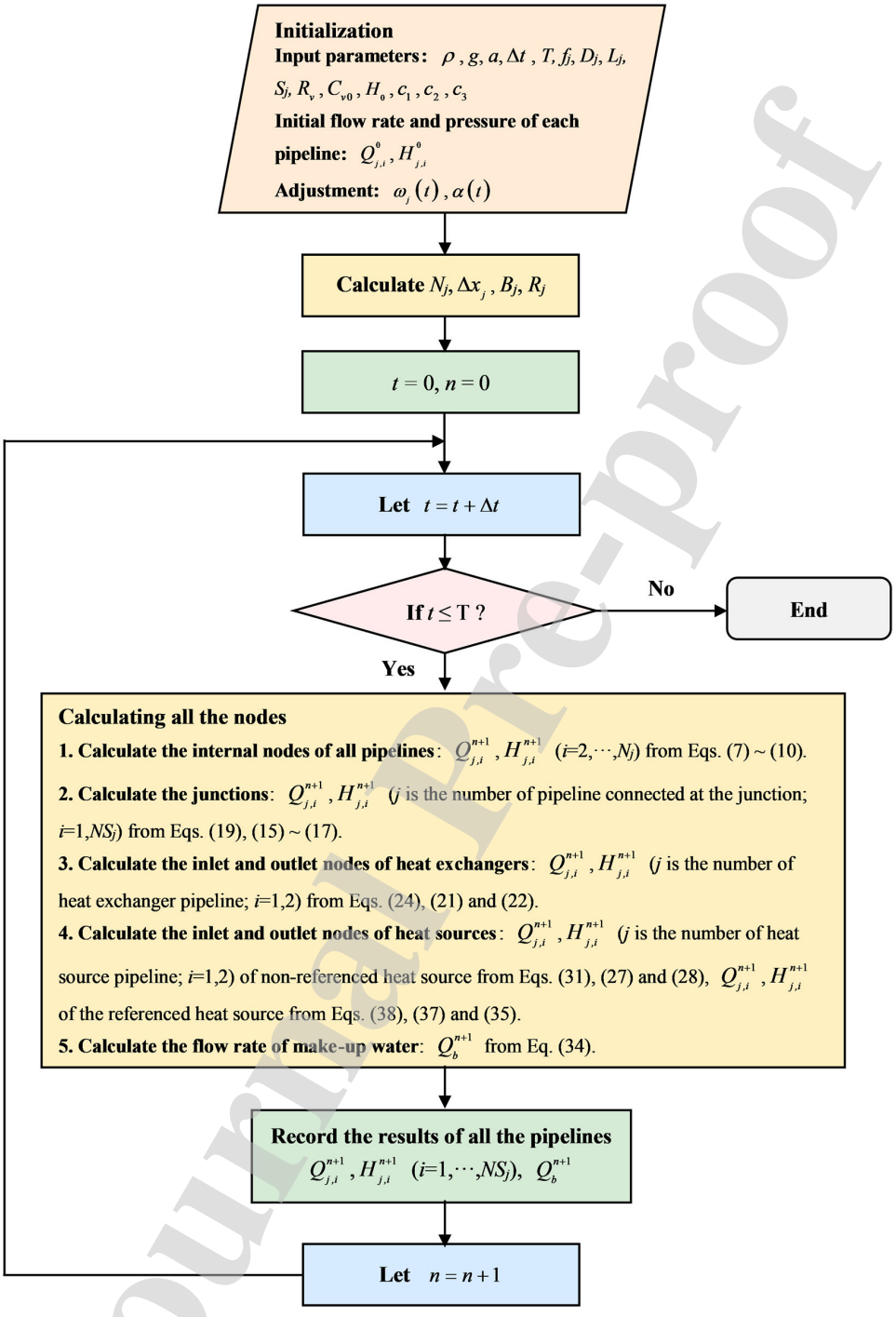

Fig. 5. Hydraulic transient calculation procedures of the DPM

2.2. Lumped parameter model

The momentum equation of the LPM is derived from Eq. (1). The pressure wave propagation and the variation of flow rate along the pipeline are neglected [12]. Only the variation of inlet and outlet pressure with t are considered, as Eq. (39).

$$\frac{\partial H}{\partial x} = -\frac{\Delta H_j}{L_j} \tag{39}$$

where ΔH (m) is the friction loss of the fluid. Substitute Eq. (39) into Eq. (1), the following equation can be obtained:

$$K_j \frac{dQ_j}{dt} = -\frac{f_j L_j}{2gD_j A_j^2} Q_j \left|Q_j\right| + \Delta H_j \tag{40}$$

where $K_j = L_j / gA_j$. The nonlinear term in Eq. (40) represents the pipeline friction loss. Eq. (40) can be extended to the following form to absorb the resistances of the heat exchangers and control valves within the heating substation and heat sources:

$$K_j \frac{dQ_j}{dt} = -S_j^* Q_j \left|Q_j\right| + \Delta H_j \tag{41}$$

where S^* is formulated as:

$$S_j^* = S_j + \phi_j + R_j N_j \tag{42}$$

According to the Kirchhoff's laws, the following matrix equations can be derived [24]:

$$B_k Q = 0 \tag{43}$$

$$C_f \Delta H^* = 0 \tag{44}$$

$$\Delta H^* = \Delta H - H_p \tag{45}$$

where B_k is the basic incidence matrix of DH network, C_f is the independent loop matrix of DH network, ΔH^* (m) is the pressure drop vector between inlets and outlets of all the pipelines, H_p (m) is the pump head vector of all circulating pumps. Q (m^3/h) is the flow rate vector of all the pipelines. Combine Eq. (41) and Eq. (44) and eliminate ΔH, the LPM of the DH network can be derived as the following form:

$$C_f diag(K)\frac{dQ}{dt} = C_f H_p - C_f diag(S^*) diag(|Q|) Q \tag{46}$$

where K, S^* and $|Q|$ are column vectors, and transformed into the following diagonal matrixes, $diag(K)$, $diag(S^*)$ and $diag(|Q|)$. Based on the graph theory, the district heating network can be considered as a connected graph. The spanning tree is defined as a subgraph of the connected graph, which can connect all the nodes of the network, but does not contain any loops. All the branches of the spanning tree are called tree branches, the remaining branches of the network are called cotree branches. Therefore, B_k and Q are partitioned into two blocks, the tree branches and the cotree branches, as Eqs. (47) and (48). Combined with Eq. (43), the flow rate vector of the tree branches can be calculated as Eq. (49) [24]. According to the relationship between the flow rate vector and the independent loop matrix, the flow rate vector can be represented by the flow rate vector of the tree branches and independent loop matrix, as Eq. (50). LPM can be obtained by substituting Eq. (50) into Eq. (46), and formulated as Eq. (51).

$$B_k = \begin{bmatrix} B_{kt} & B_{kr} \end{bmatrix} \tag{47}$$

$$Q = \begin{bmatrix} Q_t \\ Q_r \end{bmatrix} \tag{48}$$

$$Q_t = -B_{kt}^{-1} B_{kr} Q_r \tag{49}$$

$$Q = \begin{bmatrix} -B_{kt}^{-1} B_{kr} \\ I_r \end{bmatrix} Q_r = C_f^T Q_r \tag{50}$$

$$\frac{dQ_r}{dt} = (C_f diag(K) C_f^T)^{-1} C_f H_p - (C_f diag(K) C_f^T)^{-1} C_f diag(S^*) diag(\left|C_f^T Q_r\right|) C_f^T Q_r \tag{51}$$

where B_{kt} is the incidence matrix of the tree branches, B_{kr} is the incidence matrix of the cotree branches, Q_t (m^3/h) is the flow rate vector of the tree branches, Q_r (m^3/h) is the flow rate vector of the cotree branches, I_r is the identity matrix.

The fourth-order Runge-Kutta method is applied to solve Eq. (51) numerically. The form of Runge-Kutta method is written as Eqs. (52) ~ (57). The flow rate vector of the DH network can be calculated by Eq. (50).

$$Q_r^{n+1} = Q_r^n + \frac{\Delta t}{6}\left(\kappa_1 + 2\kappa_2 + 2\kappa_3 + \kappa_4\right) \tag{52}$$

$$\kappa_1 = f(Q_r^n) \tag{53}$$

$$\kappa_2 = f(Q_r^n + \frac{\Delta t}{2}\kappa_1) \tag{54}$$

$$\kappa_3 = f(Q_r^n + \frac{\Delta t}{2}\kappa_2) \tag{55}$$

$$\kappa_4 = f(Q_r^n + \Delta t \kappa_3) \tag{56}$$

$$\frac{dQ_r}{dt} = f(Q_r) \tag{57}$$

The pressure drop vector of all the pipelines can be calculated by Eqs. (41), (45), (50) and (57), as Eq. (58). And the pressures of the pipeline endpoints can be calculated by Eq. (59):

$$\Delta H^* = diag(K) C_f^T f(Q_r) + diag(S^*) diag(\left|Q\right|) Q - H_p \tag{58}$$

$$H = -B_{kt}^{-1}\Delta H^{*} + H_0 \tag{59}$$

where H here is the column vector. The detailed hydraulic transient calculation procedures of the LPM are shown in Fig. 6.

According to Eqs. (1), (2) and (41), the DPM and LPM can both degrade into Darcy friction resistance equation as Eq. (60) when steady hydraulic condition is reached, which indicates that the steady hydraulic characteristics derived by the DPM and LPM are the same.

$$\Delta H_j = S_j^{*} Q_j \left| Q_j \right| \tag{60}$$

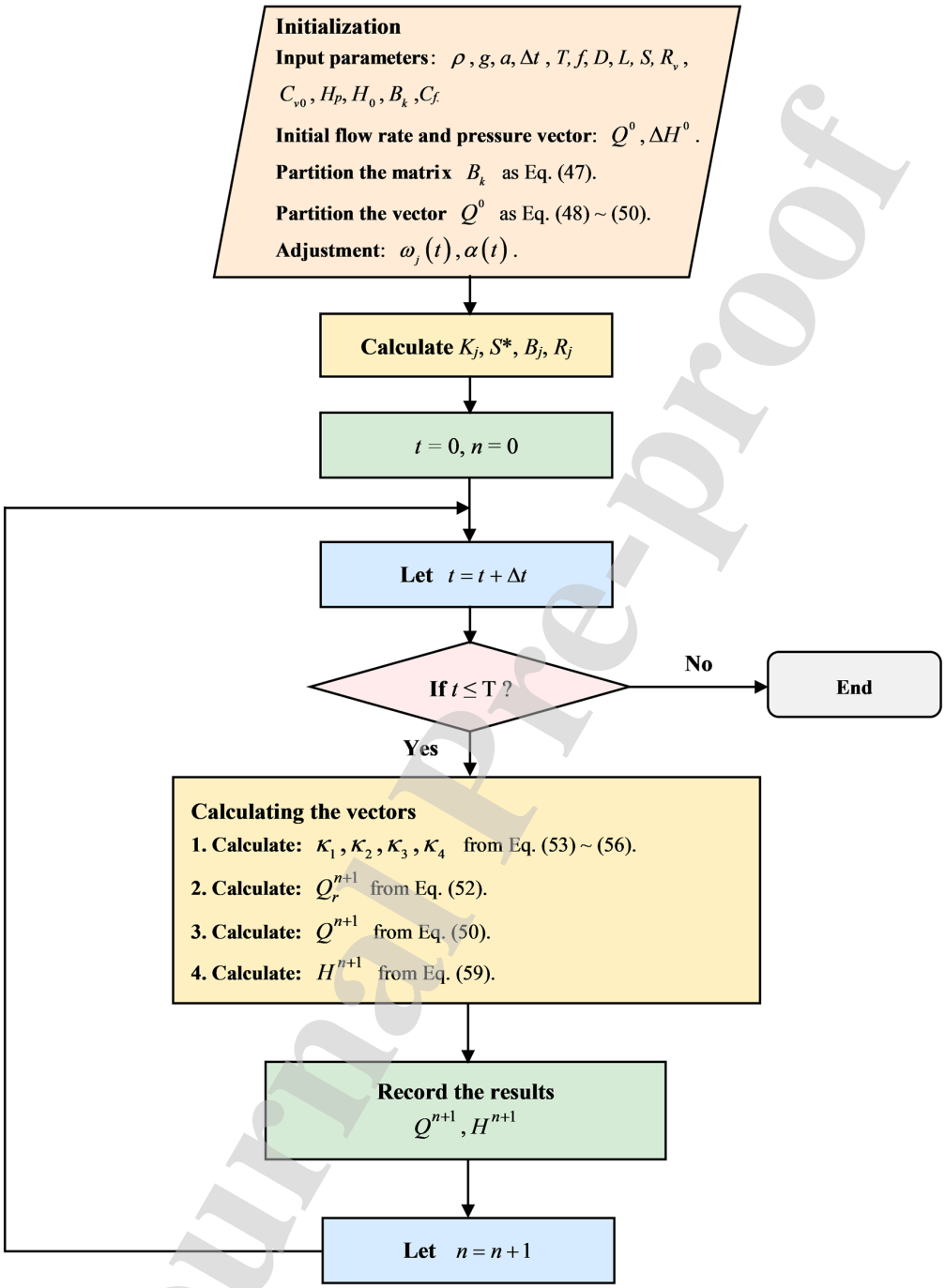

Fig. 6. Hydraulic transient calculation procedures of the LPM

3. Results and Discussion

3.1. The DH network for case study

The layout of a meshed DH network in Liaoning province is shown in Fig. 7, the red lines are cotree branches. There are 8 meshes, 3 heat sources, 72 substations and 397 pipelines. The heat source 3 is specified as the referenced heat source, whose inlet pressure head is maintained at 300kPa. The parameters of the characteristic equations of the circulating pumps at the three heat sources are listed in Table 1. Other information of the DH network can be referred from [24]. The simulations are performed on a laptop of 64bit, 4-core, 1.6GHz CPU with 8G RAM, with the Matlab software.

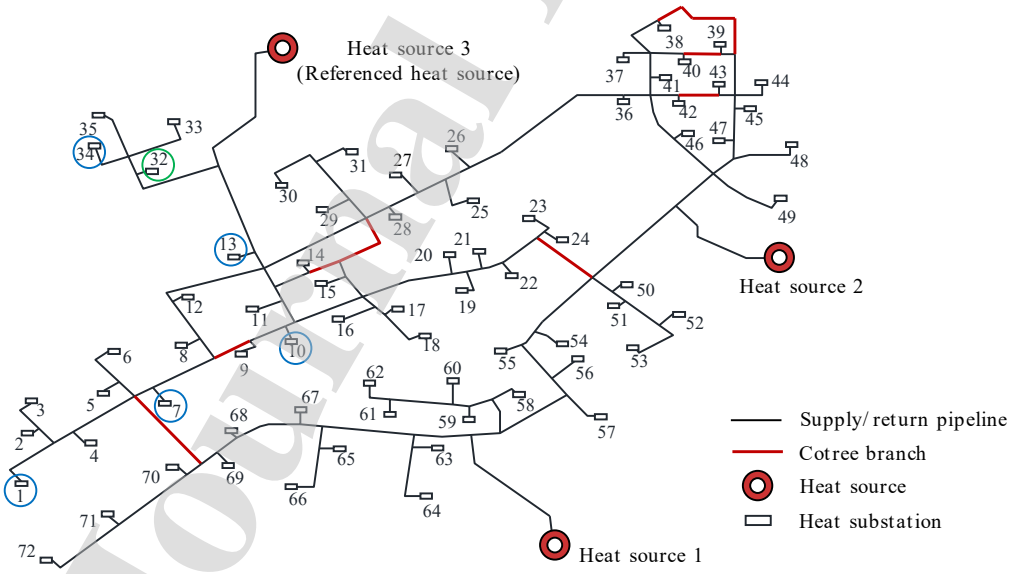

Fig. 7. Schematic of the meshed DH network layout

Table 1 Parameters of the pump characteristic equations

Number of heat source	c_1	c_2	c_3
1	-5.4688×10^{-6}	0.0119	128.00
2	-6.0000×10^{-6}	-0.0057	109.88
3	-1.5625×10^{-6}	0.0075	137.00

3.2. Spatial and time step independence tests

The simulation accuracy greatly depends on the spatial and time steps. With the increase of spatial and time steps, the computation time decreases, while the simulation accuracy becomes lower simultaneously. The purpose of the independence tests is to validate the convergence of the numerical solutions according to the decreases of the spatial and time steps, which illustrates the effectiveness of the proposed numerical methods [25].

3.2.1. Spatial and time step independence tests of the DPM

For the DPM proposed in this paper, the characteristic line method is adopted for solving the PDEs numerically, and the following relationship between the spatial and time steps should be satisfied:

$$\frac{\Delta x}{\Delta t} = a \tag{61}$$

The spatial and time steps are related by Eq. (61). The independence tests are conducted by analyzing the convergence of the numerical solutions at different scales of spatial and time steps. The following hydraulic transient process of the DH network is simulated using the DPM with $\Delta t = 0.05\text{s}$, $\Delta t = 0.02\text{s}$, $\Delta t = 0.01\text{s}$, $\Delta t = 0.005\text{s}$: the valve opening of the substation 63 is adjusted from 100% to 50% linearly within

60s from the steady state (t=0s) with the pump frequency maintained at 50Hz. The transient flow rate and pressure variations of the substation 63 are shown in Figs. 8 and 9. It is indicated that there are significant deviations between the curves of $\Delta t = 0.05\text{s}$ and the curves of other shorter time steps. The curves of $\Delta t = 0.02\text{s}$, $\Delta t = 0.01\text{s}$, $\Delta t = 0.005\text{s}$ are amplified partially in Figs. 8-b and 9-b. As is shown, with the decrease of the scale of time steps, the convergence of the flow rate and pressure curves can be observed. The simulated transient flow rate and pressure curves of $\Delta t = 0.01\text{s}$ and $\Delta t = 0.005\text{s}$ are overlapped, which indicates that the simulation accuracy is satisfactory for $\Delta t \le 0.01\text{s}$. The computation time of the DPM for simulating the 300-second real-world DH network hydraulic transients under different time steps is shown in Fig. 10. It is indicted that with the decrease of the time steps, the computation time grows exponentially. The computation time with $\Delta t = 0.005\text{s}$ is about 3 times longer than that with $\Delta t = 0.01\text{s}$, hence 0.01s is selected as the time steps of the DPM.

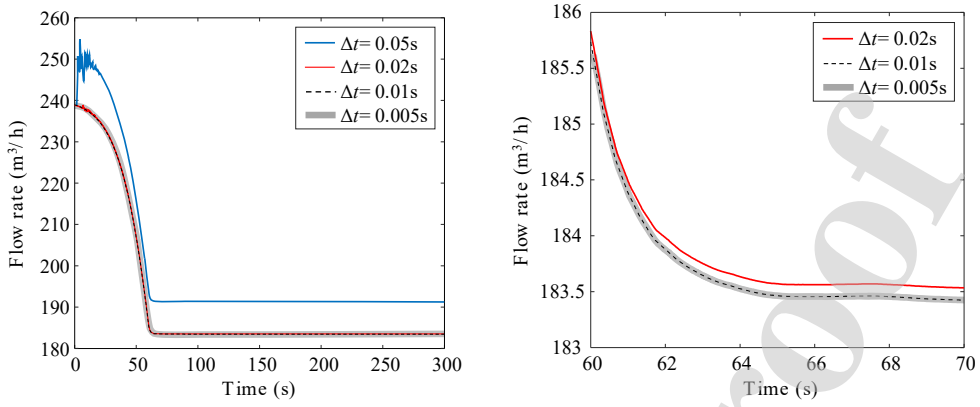

Fig. 8. Transient flow rate variations of the substation 63 under different time steps of the DPM

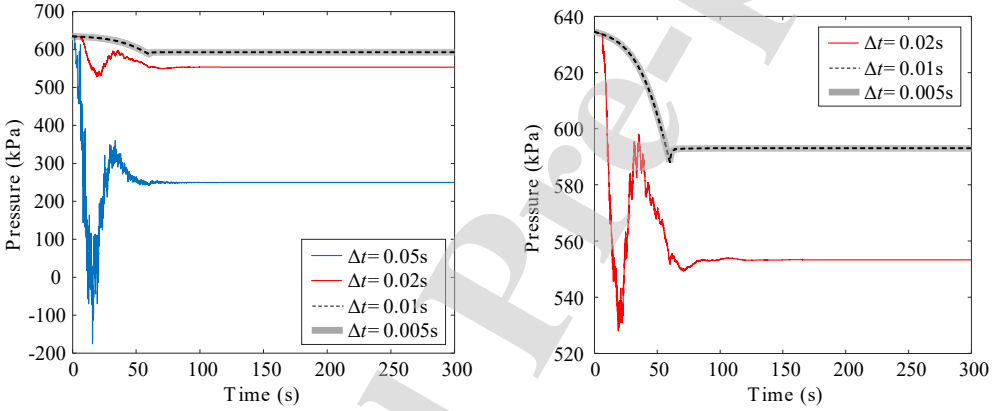

Fig. 9 Transient pressure variations of the substation 63 inlet under different time steps of the DPM

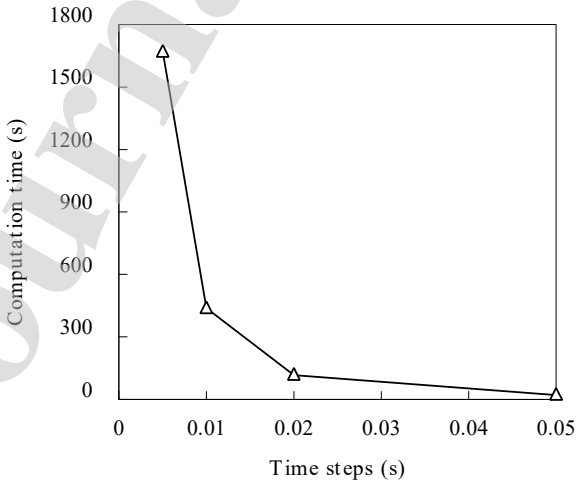

Fig. 10. Relationship between the computation time and time steps of the DPM

3.2.2. Time step independence tests of the LPM

For the LPM, its numerical stability is significantly influenced by the time steps. The time step independence tests of the LPM is conducted by analyzing the convergence of the numerical solutions to the decreased time steps. The same hydraulic transient process of the DH network is simulated using the LPM with $\Delta t = 1\text{s}$, $\Delta t = 0.5\text{s}$, $\Delta t = 0.2\text{s}$, $\Delta t = 0.1\text{s}$, $\Delta t = 0.05\text{s}$. The simulation results are shown in Figs. 11 and 12. Figs. 11-a and 12-a shows the transient flow rate and pressure variations. Figs. 11-b and 12-b shows the amplified transient curves from Figs. 11-a and 12-a. The convergences of the transient flow rate and pressure solutions can be observed with the decrease of time steps. The computation time of the LPM for simulating the 300-second real-world DH network hydraulic transients under different time steps is shown in Fig. 13. It is indicated that the computation time with $\Delta t = 0.1\text{s}$ is 52.5% shorter than that with $\Delta t = 0.05\text{s}$, hence 0.1s is selected as the time steps of the LPM.

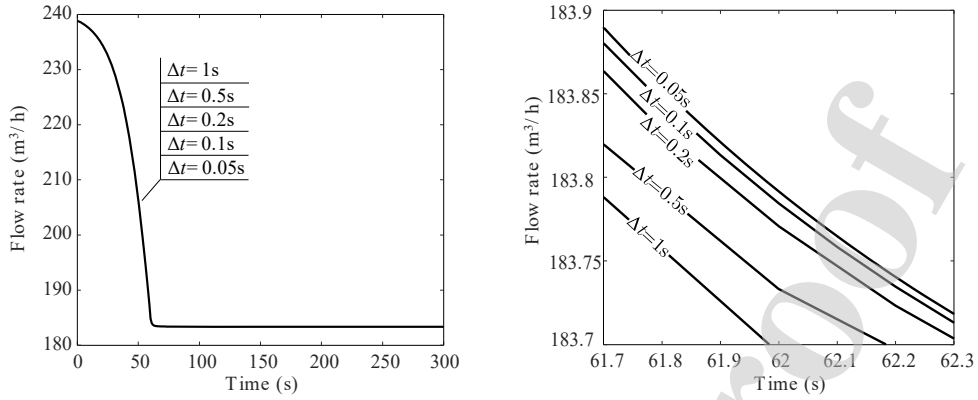

Fig. 11. Transient flow rate variations of substation 63 under different time steps of the LPM

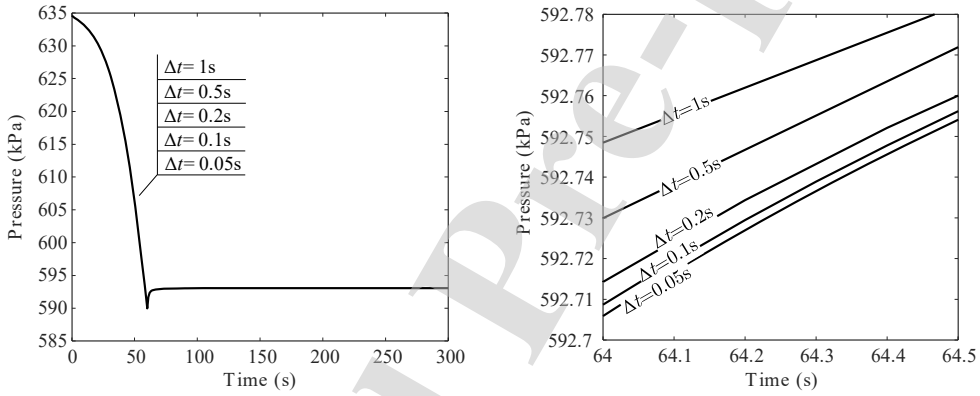

Fig. 12. Transient pressure variations of the substation 63 inlet under different time steps of the LPM

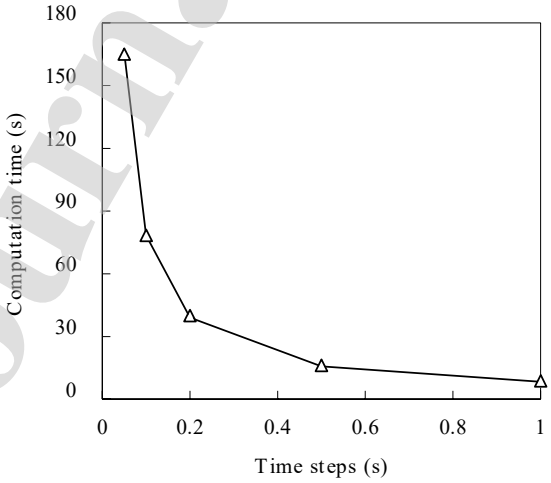

Fig. 13. Relationship between the computation time and time steps of the LPM

3.3. Hydraulic transient analysis of the DH network with the DPM and LPM

3.3.1. Substation valve opening adjustment

In this subsection, the following hydraulic transient process is simulated using the DPM and LPM: the valve opening of the substation 32 (circled in green in Fig. 7) is adjusted from 100% to 50% linearly within 60s from the steady state (t=0s) with the pump frequency maintained at 50Hz. As the valve opening decreases, the flow rate and pressure of substation 32 both undergo a hydraulic transient process from the steady states, and then reach new steady states, as shown in Fig. 14. The simulated flow rate and pressure variations obtained by the two numerical models are very close to each other. The new steady states of the two numerical solutions are also identified with each other. Local amplifications of the transient flow rate and pressure variations indicate that the high-frequency, small-amplitude hydraulic fluctuations can be captured by the DPM. But the LPM smooths these hydraulic fluctuations, due to its neglect of the pressure wave propagation along the pipelines and the elasticity of pipeline wall. Besides, it can be seen in Fig. 14-b and Fig. 14-c that the inlet pressure increases and the outlet pressure decreases, after the valve opening changes, mainly because: 1) the flow rate decreases, since the valve opening is reduced, causing the hydraulic gradient of the pipeline connected to the inlet of the substation 32 decreases, the inlet pressure of substation 32 increases; 2) as the valve opening is reduced, the local resistance of the valve increases, resulting in the decreasing of the outlet pressure of substation 32. As shown in the DPM, the amplitude of hydraulic

fluctuations of the outlet pressure at substation 32 are almost equal to that of the inlet pressure.

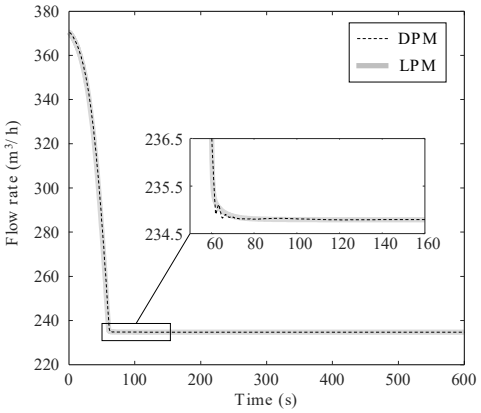

(a) Flow rate of the substation 32

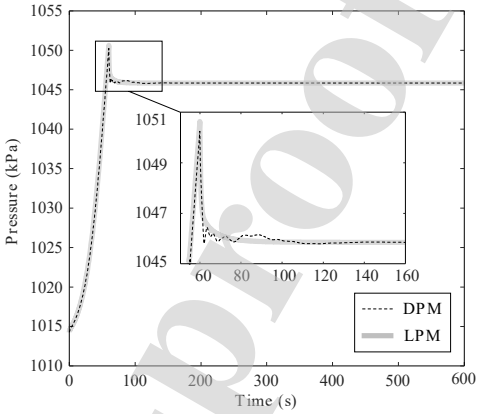

(b) Inlet pressure of the substation 32

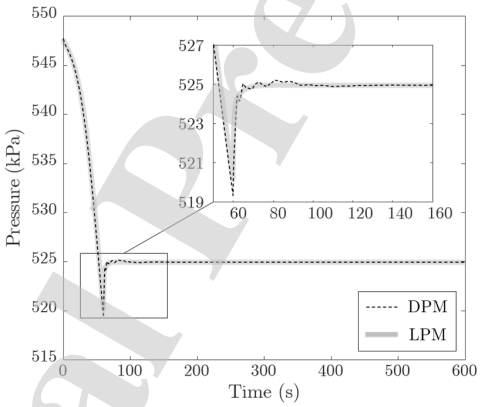

(c) Outlet pressure of the substation 32

Fig. 14. Transient flow rate and pressure variations of the substation 32 after the valve opening changes

The simulation results of the network transient flow rate and pressure variations at the substations around substation 32 (the substation 34, 13, 10, 7 and 1, which are circled in blue in Fig. 7, are selected for detailed analysis) are shown in Fig. 15. Table 2 shows the pipeline distances between these substations and the substation 32. Fig. 15 indicates that with the increase of the pipeline distance, the flow rates and

pressures reach the new steady states slower. Besides, a pure delay of the flow rate and pressure variation can be observed from the numerical results by DPM for simulating the substation different from the location where the valve opening is adjusted. And the pure delay enlarges with the increase of pipeline distance. The pure delay approximately equals the quotient of the pipeline distance and the pressure wave velocity, which indicates that the influence of the valve opening adjustment on the hydraulic conditions propagates through the pipelines in the DH network at the speed of pressure wave. As the pipeline distance from the substation 32 increases, the pure delay gets larger, and the hydraulic transient processes illustrated by DPM and LPM are more different. Due to the omitting of the propagation and attenuation of pressure wave in LPM, there is no delay in the solutions of the LPM. The flow rates and pressures of these substations change immediately at the beginning of the adjustment, regardless of the pipeline distance from the substation 32.

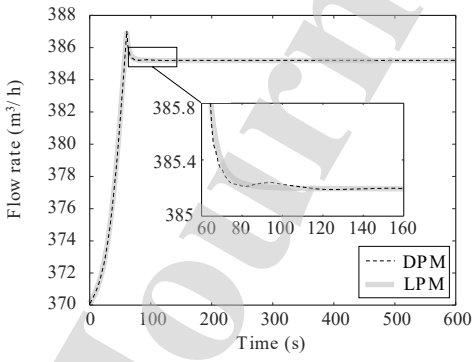

(a) Flow rate of the substation 34

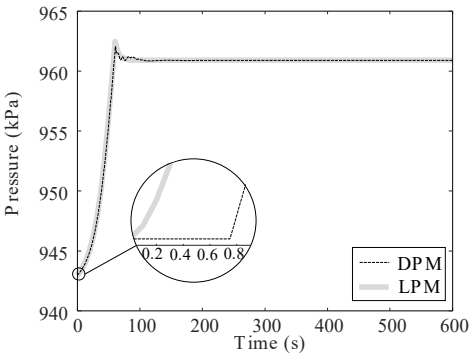

(b) Inlet pressure of the substation 34

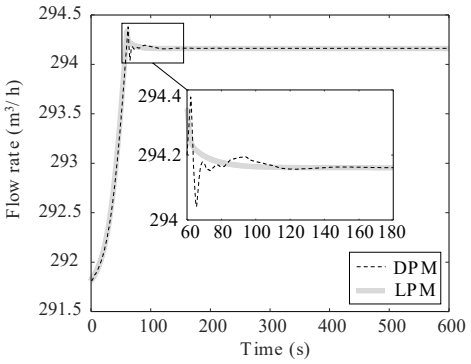

(c) Flow rate of the substation 13

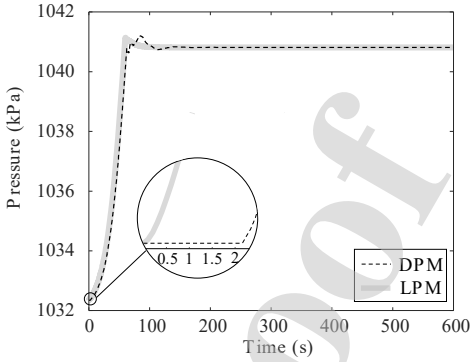

(d) Inlet pressure of the substation 13

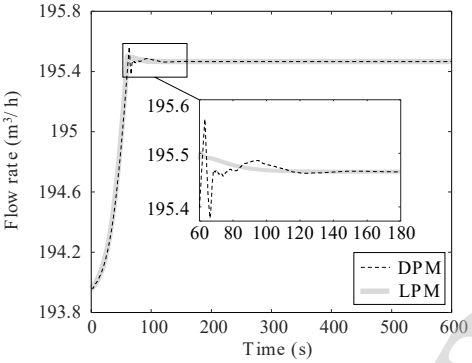

(e) Flow rate of the substation 10

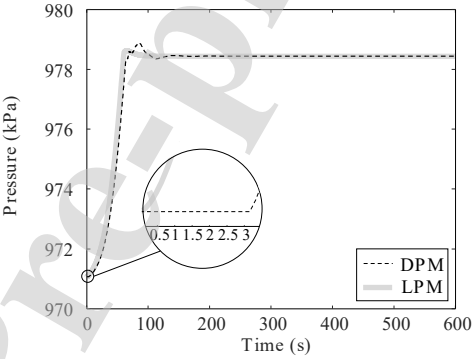

(f) Inlet pressure of the substation 10

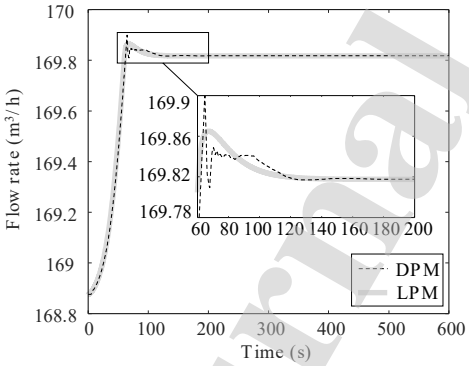

(g) Flow rate of the substation7

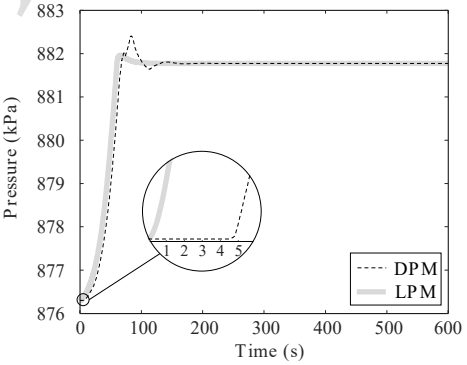

(h) Inlet pressure of the substation 7

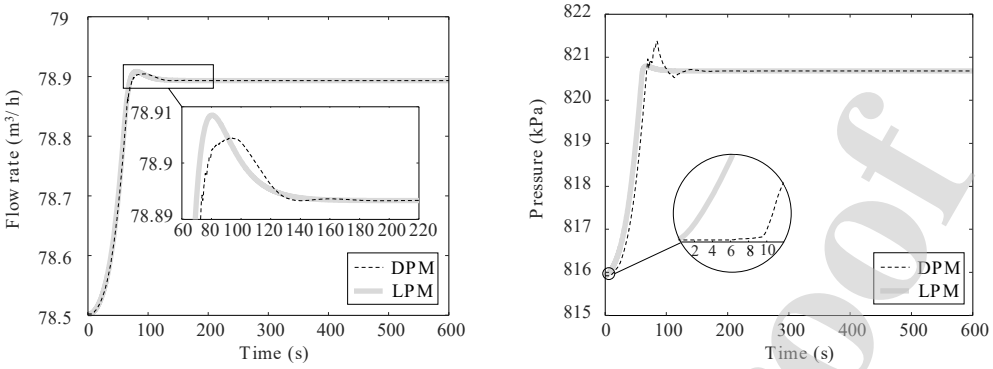

(i) Flow rate of the substation 1 (j) Inlet pressure of the substation 1

Fig. 15. Transient flow rate and pressure variations of the substations after the valve opening changes

Table 2 Pure delay of the substation flow rate and pressure

Substation	Pipeline distance from the substation 32 (m)	Pure delay (s)
34	743	0.8
13	2284	2.2
10	3269	3.2
7	4659	4.6
1	6209	6.1

As shown in Fig. 16, the hydraulic transients at the referenced heat source are more severe than those at other heat sources and substations. The flow rates and pressures of the non-referenced heat sources increase slightly, while the flow rate and pressure of the referenced heat source drops by 46 m^3/h and increases by 9 kPa, respectively. The flow rate and pressure of the referenced heat source reach the new steady states at 205s, nearly 50s later than that of the substation 32. The high-frequency hydraulic fluctuations of the referenced heat source simulated by DPM are obvious than those of the substation 32, the maximum fluctuation range is within 2 m^3/h and 1 kPa for flow rate and pressure, respectively. The simulated

hydraulic responses of the three heat sources by the DPM also have pure delays with respect to the adjusted substation. The pure delay of the flow rate and pressure responses of the referenced heat source, heat source 2 and 1 are 2.6s, 8.2s and 9.6s, respectively. The pure delay and the pipeline distance from substation 32 are positively correlated. As the distance between the heat source and substation 32 increases, the hydraulic transients simulated by DPM are much different from those simulated by LPM, since the influence of pressure wave propagation on hydraulic transient characteristics becomes more significant.

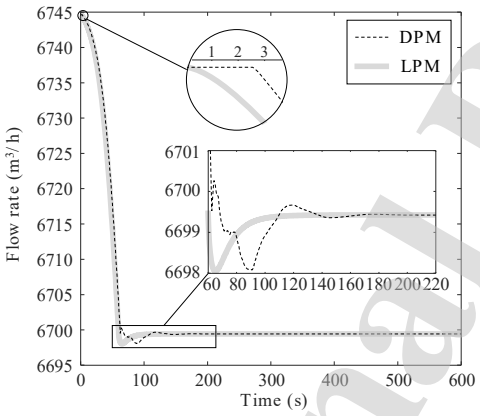

(a) Flow rate of the referenced heat source

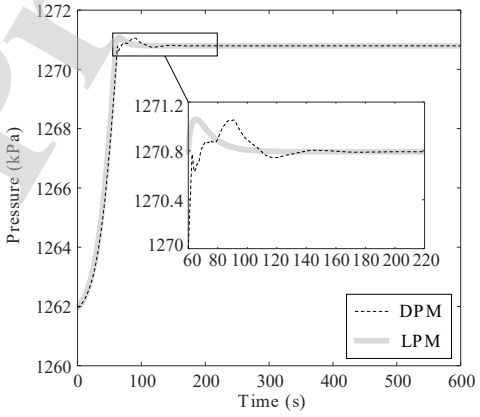

(b) Outlet pressure of the referenced heat source

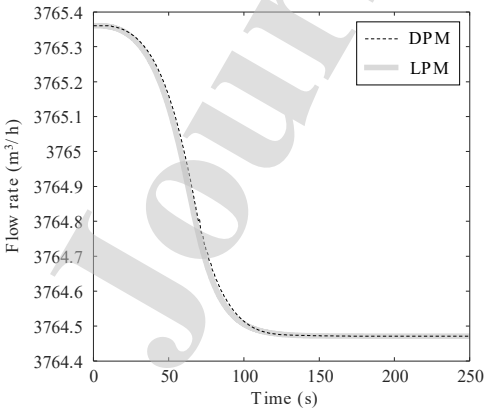

(c) Flow rate of heat source 1

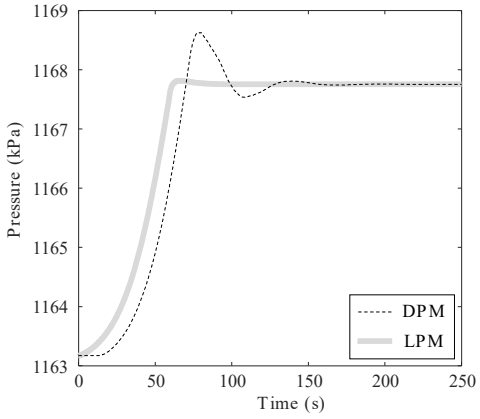

(d) Outlet pressure of heat source 1

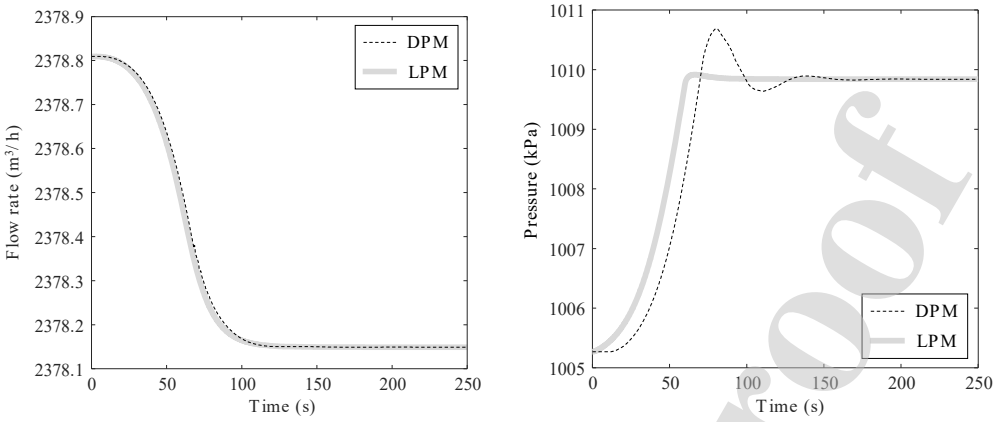

(e) Flow rate of heat source 2 (f) Outlet pressure of heat source 2

Fig. 16. Transient flow rate and pressure variations of three heat sources after the valve opening changes

To analyze the influence of adjustment durations on hydraulic transients of DH network, the following transient hydraulic processes are simulated with the DPM and LPM: the valve opening of substation 32 is adjusted from 100% to 50% linearly within 30s and 5s from the steady state (t=0s) with the pump frequency maintained at 50Hz. As shown in Fig. 17, when the adjustment duration of the valve opening in substation 32 is 60s, 30s and 5s, the transient time for the flow rates and pressures reaching the new steady states is 95s, 109s and 123s, respectively. It is indicated that with the decrease of the adjustment duration of the valve opening, the transient time for the flow rates and pressures reaching the new steady states gets longer. With the decrease of the adjustment duration of the valve opening, high-frequency signals of the valve opening variations are introduced, hence high-frequency hydraulic transients will be observed, as shown in the simulated results by the DPM. The frequency and amplitude of hydraulic fluctuations both increase with the reduction of the adjustment duration. However, the LPM still cannot capture the high-frequency hydraulic

fluctuations, with the decrease of the adjustment duration. As shown in Table 3, the transient time of the substation flow rates and pressures reaching the new steady states for the adjustment duration within 30s and 5s are generally 20.4% and 38.6% longer than that for the adjustment duration within 60s.

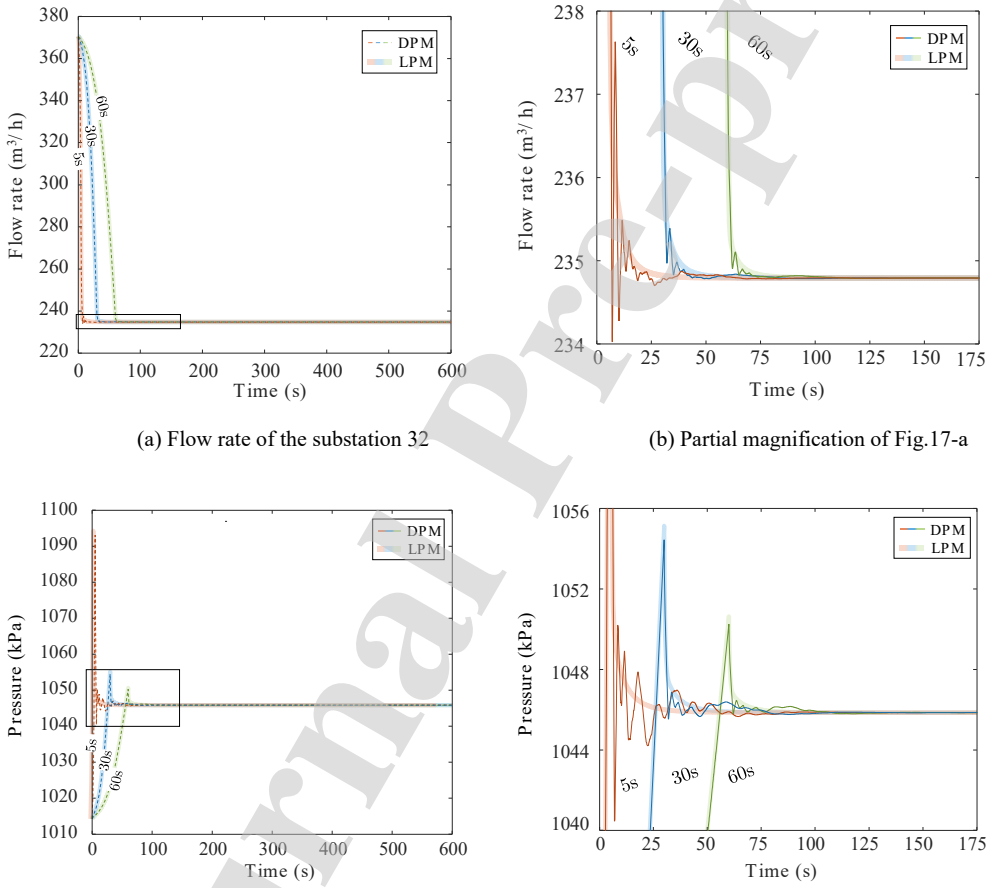

(a) Flow rate of the substation 32

(b) Partial magnification of Fig.17-a

(c) Inlet pressure of the substation 32

(d) Partial magnification of Fig.17-c

Fig. 17. Transient flow rate and pressure variations of the substation 32 for the valve opening adjustment duration within 60s, 30s and 5s

Table 3 Transient time for substation flow rate and pressure reaching the new steady states under the valve opening adjustment duration within 60s, 30s and 5s

Substation	Adjustment duration

	60s	30s	5s
34	102.9s	130s	155s
13	110.6s	133.3s	167.3s
10	129.9s	161.3s	179.1s
7	147.1s	170.7s	191.7s
1	159.2s	182.7s	195.7s

When adjusting the substation valve opening, the flow rates and pressures fluctuate obviously at all the nodes of the pipelines. Due to the compressibility of the fluid and the elasticity of the pipeline wall, the fluid is compressed and the pipeline wall is expended because of the increased pressure of the pipeline. Therefore, the make-up water is required to ensure the constant pressure at the circulating pump inlet of the referenced heat source. Since the LPM neglects the compressibility of the fluid and the elasticity of the pipes, if the network doesn't have any leakage points, the flow rate of the make-up water simulated by the LPM will always be zero. Nevertheless, the transient flow rates of the constant pressure replenishment system can be simulated by DPM. The simulations are conducted with three different adjustment durations, 60s, 30s and 5s, for the substation 32 valve opening adjustment. As shown in Fig. 18, the flow rates of the constant pressure make-up water are zero initially, and start to increase at 2.6s, which shows the pure delays to the adjustment of the substation 32 valve opening. The first peaks of the flow rate fluctuations all occur at the 2.6s after the end of the adjustments for the three cases, and the peak values are 9.6 m^3/h, 16.1 m^3/h and 27.7 m^3/h, respectively, for the adjustment durations of 60s, 30s and 5s. For the adjustment duration of 5s, a second peak of the flow rate

fluctuations occurs at 16.5s after the first peak, and the amplitude of the second peak is 45.8% lower than that of the first peak. The flow rates decrease gradually after the peaks, then returns to zero in 80s, 81.7s and 87.5s after the end of the adjustment, for the adjustment durations of 60s, 30s and 5s, respectively.

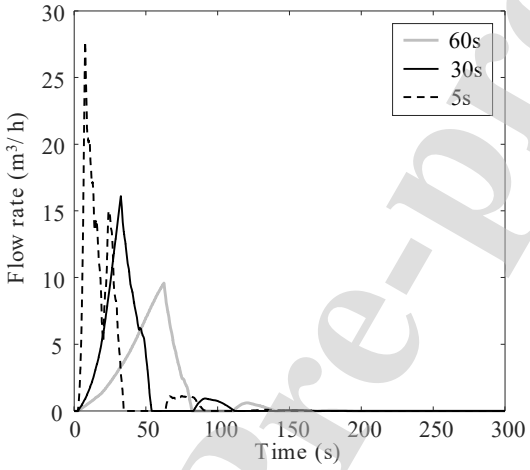

Fig. 18. Transient flow rate variations of the make-up water for the valve opening adjustment duration within 60s, 30s and 5s

3.3.2. Heat source circulating pump frequency adjustment

In this subsection, the hydraulic transients introduced by the heat source circulating pump frequency adjustment are analyzed. The following hydraulic transient processes of the DH network are simulated: the pump frequency of the referenced heat source is adjusted from 50Hz to 25Hz linearly in 60s from the steady state (t=0s) with all substation valve openings maintained at 100%. As shown in Fig. 19, the steady hydraulic characteristics after the adjustment simulated by DPM and LPM are identified with each other. As the flow rate of the referenced heat source decreases by 51.1%, the flow rate of the heat source 1 and 2 only increases by 1% and

1.5%. The pressures of heat source 1 and 2 changes greatly compared with the flow rate, which drops by 31.3% and 36.4%. The flow rate and pressure of the referenced heat source, heat source 1 and 2 reach the new steady states in 160s, 260s and 250s after the end of adjustment, which are much longer than those for adjusting valve opening. When adjusting pump frequency, the frequency and amplitude of hydraulic fluctuations from 60s to the new steady state simulated by DPM are higher than that for adjusting valve opening, the maximum fluctuation ranges of the referenced heat source are within 180 m^3/h and 50kPa for the flow rate and pressure, respectively. As simulated by DPM, the flow rate and pressure variations of the heat source 1 and 2 both have pure delays. In addition, the hydraulic transient processes illustrated by DPM and LPM are slightly different after 0s, the pure delay and hydraulic transients induced by the propagation of the pressure waves are more obvious, especially for the heat source 1, which is further from the referenced heat source.

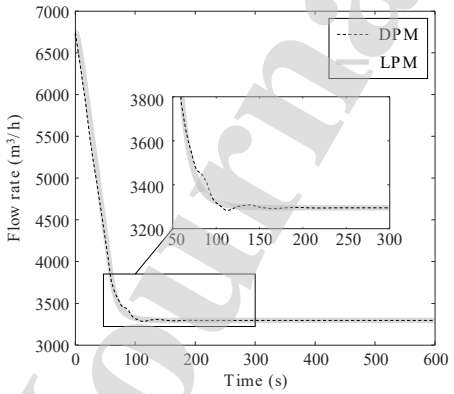

(a) Flow rate of the referenced heat source

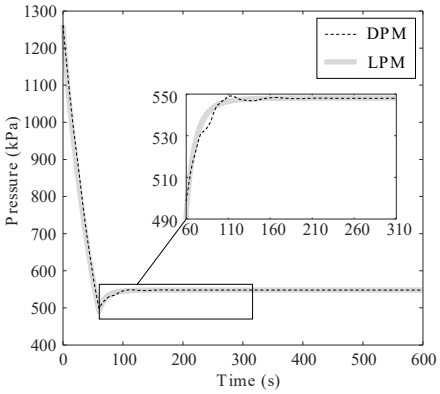

(b) Outlet pressure of the referenced heat source

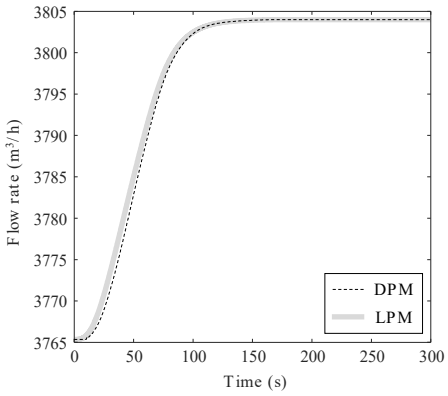

(c) Flow rate of heat source 1

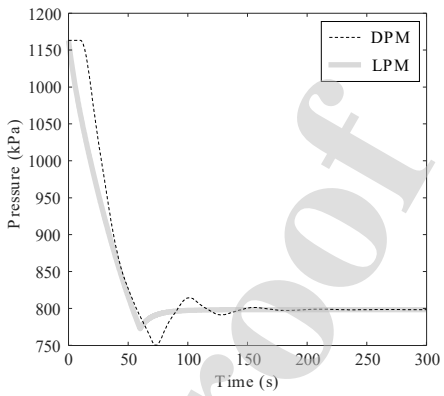

(d) Outlet pressure of heat source 1

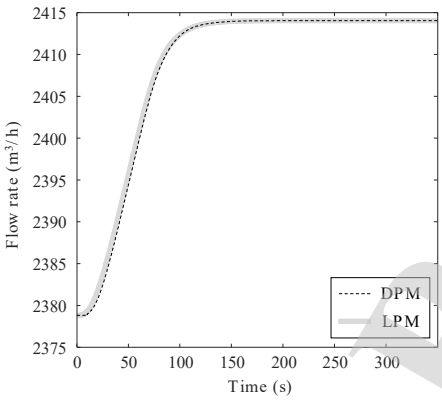

(e) Flow rate of heat source 2

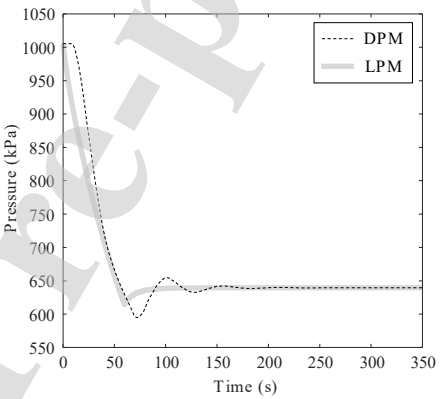

(f) Outlet pressure of heat source 2

Fig. 19. Transient flow rate and pressure variations of three heat sources after the pump frequency changes

When adjusting the pump frequency, the variation amplitudes of the substation flow rates and pressures are larger than those for adjusting valve opening, as shown by the simulation results of DPM and LPM in Fig. 20. The flow rates and pressures of these substations decrease by 43.1% and 49.7% on average when adjusting the heat source pump frequency, while the flow rates and pressures vary only 0.66% and 0.75% when adjusting the substation valve openings. The transient time for the substation flow rates and pressures reaching the new steady states are averagely 46.6% longer

than those for adjusting valve openings. With the increase of the pipeline distances between the referenced heat source and these substations, the transient time for the substation flow rates and pressures reaching the new steady states vary from 150s to 220s. The pure delay of the substation flow rate and pressure response to the pump frequency adjustment can be observed from the numerical results by DPM. Due to the pure delay, the deviations between the curves of hydraulic transient processes illustrated by DPM and LPM enlarge with the increase of the pipeline distance from the referenced heat source. When adjusting the pump frequency, the differences between the simulation results of the transient flow rates and pressures obtained by DPM and LPM become more obvious than those for adjusting the substation valve openings.

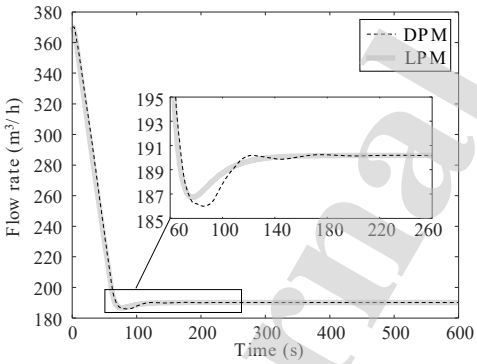

(a) Flow rate of the substation 34

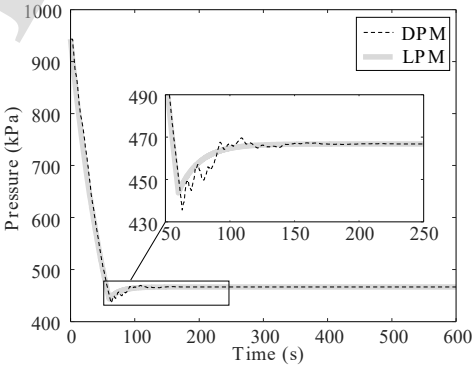

(b) Inlet pressure of the substation 34

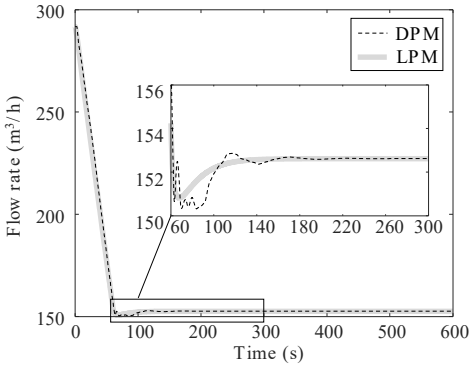

(c) Flow rate of the substation 13

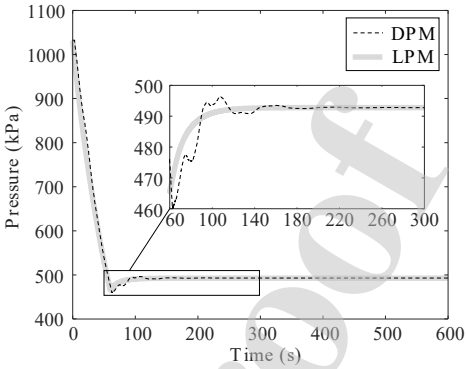

(d) Inlet pressure of the substation 13

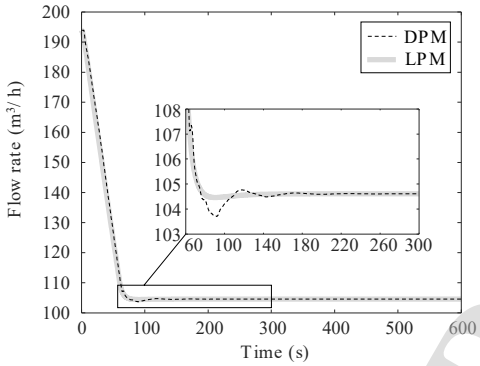

(e) Flow rate of the substation 10

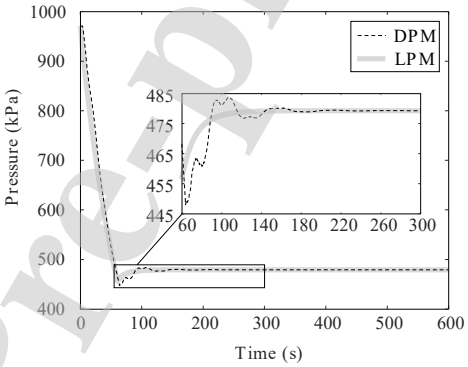

(f) Inlet pressure of the substation 10

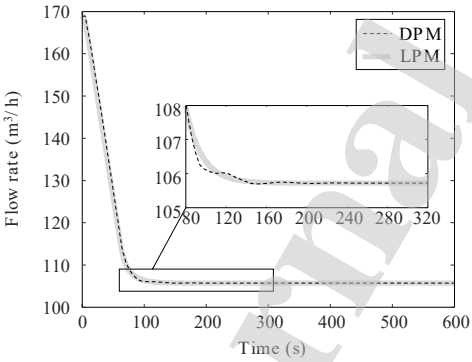

(g) Flow rate of the substation 7

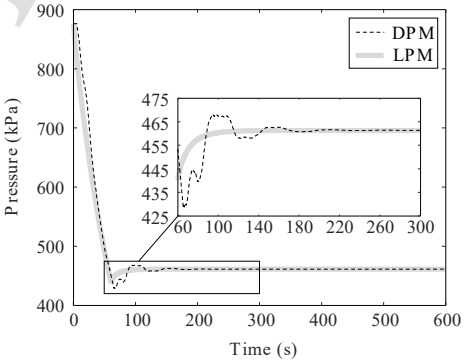

(h) Inlet pressure of the substation 7

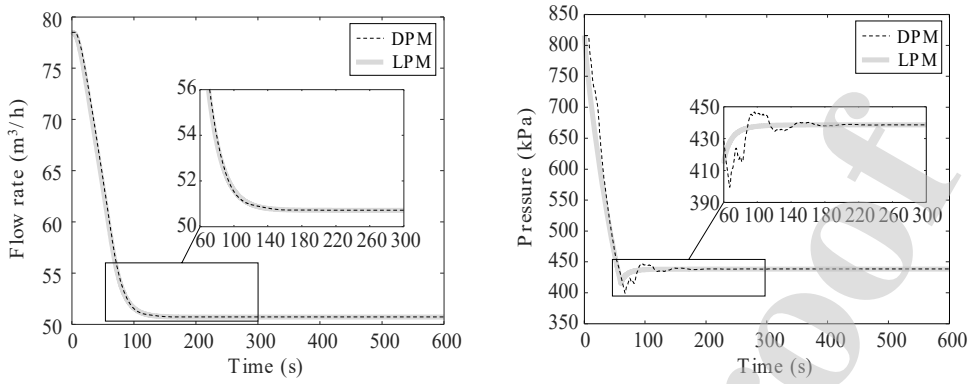

(i) Flow rate of the substation 1

(j) Inlet pressure of the substation 1

Fig. 20. Transient flow rate and pressure variations of the substations after the pump frequency changes

With the decrease of the adjustment duration, the transient time for substation flow rate and pressure reaching the new steady states increases after the pump frequency changes. The tranisent flow rate and pressure variations of the referenced heat source are shown in Fig. 21. With the decrease of the adjustment duration, the diffrences between the simulation results of tranisent flow rates and pressures illustrated by DPM and LPM get larger, and the high-frequency hydraulic fluctuations from the end of adjustment to the new steady state observed by the DPM become more drastic, whose range is within 457m^3/h and 442kPa for the adjustment duration within 30s. As shown in Table 4, the transient time for substation flow rate and pressure reaching the new steady states for the adjustment duration within 30s is 20.8% and 36.1% longer than that for the adjustment duration within 60s and 120s. It is indicated that the transient time for flow rate and pressure reaching the new steady states is generally longer than that for adjusting valve openings.

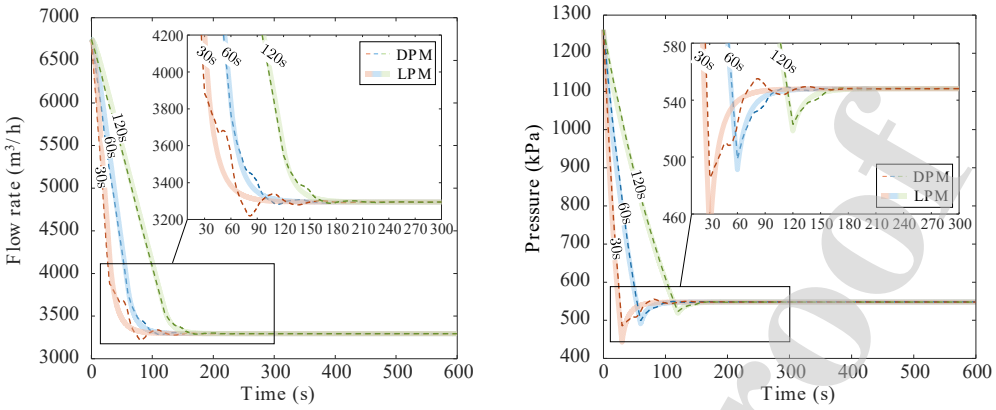

(a) Flow rate of the referenced heat source

(b) Outlet pressure of the referenced heat source

Fig. 21. Transient flow rate and pressure variations of the referenced heat source under the pump frequency adjustment duration within 120s, 60s and 30s

Table 4 Transient time for the substation flow rates and pressures reaching new steady states under the pump frequency adjustment duration within 120s, 60s and 30s

Substation	Adjustment duration		
	120s	60s	30s
34	129.6s	158.2s	192.8s
13	153.7s	162.8s	194.7s
10	168.2s	191.3s	238s
7	193.3s	215.6s	250.9s
1	198.6s	218.1s	265.7s

The simulations of the constant pressure replenishment system are conducted by the DPM for the pump frequency adjustment under three different adjustment durations, 120s, 60s and 30s. As shown in Fig. 22, the peak flow rates of make-up water are 80.8 m^3/h, 146.4 m^3/h and 519.8 m^3/h for the adjustment duration within 120s, 60s and 30s, which are significantly higher than those for the valve opening adjustment, mainly because the fluid is compressed and the pipeline wall is expended more greatly after the pump frequency changes than that after the valve opening changes. The first peaks generally occur at 112.6s, 67.5s, 10.5s after the end of the

adjustment for the adjustment duration within 120s, 60s and 30s. The flow rate gradually decreases after the last peak, then returns to zero at 206.1s, 212s and 259.9s after the end of the adjustment. It is indicated that as the adjustment duration decreases, the transient time for flow rates reaching the new steady states increases, and the transient time is generally much longer than that for adjusting the valve opening.

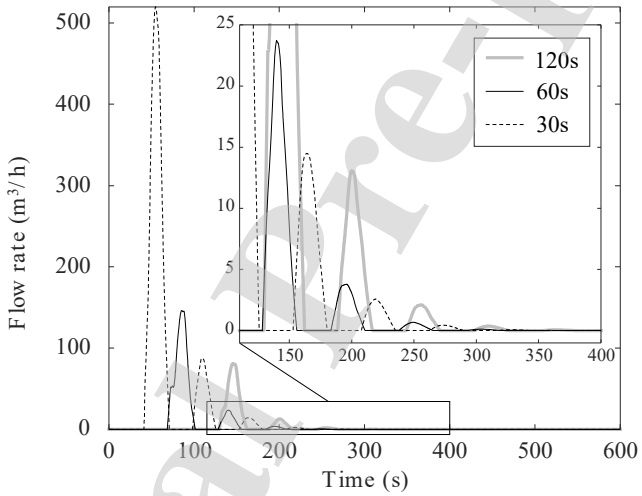

Fig. 22. Transient flow rate variations of the make-up water for the pump frequency adjustment duration within 120s, 60s and 30s

The computation time of a 600-second real-world DH network hydraulic transient process is shown in Table 5. If all the data of each time and spatial step is recorded, the computation time of LPM is 81.5% shorter than that of DPM, mainly because: 1) the variation of flow rate with axial length is not considered by LPM; 2) only inlet and outlet pressure of pipelines are simulated in LPM; 3) the data can be vectorized when simulating by LPM. The equations of the characteristic lines and the

boundary conditions of the DPM are not easy to be vectorized, hence the simulation is done node by node of each pipeline, and then time step by time step. As the simulation proceeds, large amounts of data need to be recorded, the memory footprint becomes larger, which causes the simulation of DPM to be significantly slower than the real-world DH network hydraulic transient process. However, if the data of inlet and outlet pressure and flow rate of each pipeline, just like the data recorded by LPM, is recorded at every time step in DPM, the computation time of DPM can be reduced by 78.8% compared with that for recording all the data. In fact, the hydraulic transients of the substations and heat sources are more concerned. If the data of substations and heat sources is recorded, the computation time of DPM can be reduced by 85.1% compared with that for recording all the data.

Table 5 Computation time of the DPM and LPM in different conditions

Model	DPM			LPM
	Record all the data	Record the data of inlet and outlet pressure and flow rate of each pipeline	Record the data of substations and heat sources	Record all the data
Amount of data recorded	60001×24024	60001×1192	60001×226	6001×1192
Computation time (s)	852.6	181.2	127.1	158

4. Conclusions

In this paper, the DPM and LPM of DH network were established, the numerical methods were introduced. The DPM and LPM were both applied to a meshed DH network with multiple heat sources for simulation analysis of hydraulic transients, the

comparison between the simulation performances of the two models was conducted. The main conclusions were summarized as follows:

(1) The DPM and LPM can both be applied to analyze the unsteady hydraulic response. As the pipeline distances from adjustment location, the transient time for the flow rate and pressure reaching the new steady states gets longer. As the adjustment duration decreases, the transient time for flow rate and pressure reaching the new steady states increases. When adjusting the pump frequency, the transient time for flow rate and pressure reaching the new steady states is much longer than that for adjusting the substation valve opening.

(2) The high-frequency hydraulic transient characteristics can be captured by DPM subtly. With the decrease of adjustment duration, more severe high-frequency hydraulic transients will occur. When adjusting pump frequency, the high-frequency hydraulic transient characteristics became more obvious than that for adjusting the valve opening. However, only the average hydraulic fluctuations can be described by LPM.

(3) The pure delay for the flow rate and pressure response to the adjustment can be observed by DPM. As the pipeline distances from the adjustment location increase, the pure delays increase accordingly, which indicates that the influence of the adjustment on the hydraulic conditions propagates through the pipelines in the DH network at the speed of pressure wave.

(4) It is indicated by the simulation results of the DPM that as the adjustment

duration decreases, the flow rate of the constant pressure make-up water increases. When adjusting pump frequency, the peak flow rates of the make-up water are greatly higher than those for adjusting valve opening, and the transient time for the flow rates reaching the new steady state gets longer.

(5) The computation time of LPM is shorter than DPM because of the vectorizable calculation procedure and the less data to record due to the neglect of the pressure wave propagation and the compressibility of the fluid in LPM. If the data of inlet and outlet pressure and flow rate of each pipeline is recorded, the computation time of DPM can be reduced by 78.8% compared with that for recording all the data.

(6) In the further study, the DPM can be applied to the water hammer protection and the rapid leakage detection of the large-scale district heating networks based on its accurate simulation of hydraulic transient characteristics including the propagation of pressure wave and high-frequency hydraulic fluctuations.

Acknowledgements

This work was supported by the Natural Science Foundation of Tianjin [No. 19JCQNJC07200] and the National Key R&D Program of China [No. 2018YFC0705000].

References

[1] H. Lund, N. Duic, P.A. Østergaard, B.V. Mathiesen, Future district heating systems and

technologies: On the role of smart energy systems and 4th generation district heating, Energy, 165 (2018) 614-619. https://doi.org/10.1016/j.energy.2018.09.115.

[2] Y. Wang, Research on Dynamic Characteristic Analysis and Robust Optimal Control of District Heating System, Doctor, Tianjin University, 2017.

[3] V.D. Stevanovic, S. Prica, B. Maslovaric, B. Zivkovic, S. Nikodijevic, Efficient numerical method for district heating system hydraulics, Energy Convers. Manage. 48 (5) (2007) 1536-1543. https://doi.org/10.1016/j.enconman.2006.11.018.

[4] S. Zhou, H. Li, T. Wang, P. Gong, A Novel Hydraulic Simulation Platform of Multi-source and Multi-ring Experimental Heating Network, Procedia Engineering, 205 (2017) 2063-2068. https://doi.org/10.1016/j.proeng.2017.10.093.

[5] S. Zhou, H. Li, P. Gong, M. Tian, Hydraulic modeling of double-source and ring-shaped heating networks, Appl. Therm. Eng. 119 (2017) 215-221. https://doi.org/10.1016/j.applthermaleng.2017.03.035.

[6] S. Zhou, P. Gong, T. Wang, H. Li, Hydraulic modeling and experimental study of three heat sources and three rings heating networks, Procedia Engineering, 205 (2017) 2670-2676. https://doi.org/10.1016/j.proeng.2017.10.220.

[7] H. Wang, H. Wang, H. Zhou, T. Zhu, Modeling and optimization for hydraulic performance design in multi-source district heating with fluctuating renewables, Energy Convers. Manage. 156 (2018) 113-129. https://doi.org/10.1016/j.enconman.2017.10.078.

[8] E. Gong, N. Wang, S. You, Y. Wang, H. Zhang, S. Wei, Optimal operation of novel hybrid district heating system driven by central and distributed variable speed pumps, Energy Convers. Manage. 196 (2019) 211-226. https://doi.org/10.1016/j.enconman.2019.06.004.

[9] E. Guelpa, C. Toro, A. Sciacovelli, R. Melli, E. Sciubba, V. Verda, Optimal operation of large district heating networks through fast fluid-dynamic simulation, Energy, 102 (2016) 586-595. https://doi.org/10.1016/j.energy.2016.02.058.

[10] C.D. Persis, T.N. Jensen, R. Ortega, R. Wisniewski, Output Regulation of Large-Scale Hydraulic Networks, IEEE Transactions on Control Systems Technology, 22 (1) (2014) 238-245. http://dx.doi.org/10.1109/TCST.2012.2233477.

[11] J. Hua, S. Zhang, L. Fu, Similitude criterion derivation and pipe physical property test and

suitable analysis for water hammner scale model of long distance district heating pipeline, Appl. Therm. Eng., 125 (2017) 80-90. https://doi.org/10.1016/j.applthermaleng.2017.07.013.

[12] S. You, L. Mi, Y. Wang, H. Zhang, X. Zheng, W. Zheng, Unsteady Hydraulic Modeling and Dynamic Response Analysis of a District Heating Network, Journal of Tianjin University(Science and Technology) 52 (08) (2019) 849-856. https://dx.doi.org/10.11784/tdxbz201808091.

[13] D. Wood, P. Boulos, B. Karney, D. McPherson, S. Lingireddy, Numerical methods for modeling transient flow in distribution systems, Journal - American Water Works Association, 97 (2005) 104-115. https://doi.org/10.1002/j.1551-8833.2005.tb10936.x.

[14] K.A. Pambour, R. Bolado-Lavin, G.P.J. Dijkema, An integrated transient model for simulating the operation of natural gas transport systems, J. Nat. Gas Sci. Eng. 28 (2016) 672-690. https://doi.org/10.1016/j.jngse.2015.11.036.

[15] B. Karney, D. McInnis, Transient Analysis of Water Distribution Systems, Journal - American Water Works Association, 82 (1990) 62-70. http://doi.org/10.1002/j.15518833.1990.tb06992.x.

[16] H.J. Kwon, Computer simulations of transient flow in a real city water distribution system, KSCE J. Civ. Eng. 11 (1) (2007) 43-49. https://doi.org/10.1007/BF02823371.

[17] M. Fathi-Moghadam, S. Kiani, Simulation of transient flow in viscoelastic pipe networks, J. Hydraul. Res. (2019) 1-10. https://doi.org/10.1080/00221686.2019.1581669.

[18] M.H. Chaudhry, Applied Hydraulic Transients, Springer, New York, 2014.

[19] H.J. Kwon, J.-J. Lee, Computer and experimental models of transient flow in a pipe involving backflow preventers, J. Hydraul. Eng. 134 (4) (2008) 426-434. https://doi.org/10.1061/(ASCE)0733-9429(2008)134:4(426).

[20] E.B. Wylie, V.L. Streeter, L. Suo, Fluid Transients in Systems, Prentice Hall, 1993.

[21] A. Kaliatka, M. Vaišnoras, M. Valinčius, Modelling of valve induced water hammer phenomena in a district heating system, Computers & Fluids, 94 (2014) 30-36. https://doi.org/10.1016/j.compfluid.2014.01.035.

[22] B. Brunone, Transient Test-Based Technique for Leak Detection in Outfall Pipes, Journal of Water Resources Planning and Management, 125 (5) (1999) 302-306.

https://doi.org/10.1061/(ASCE)0733-9496(1999)125:5(302).

[23] E.B. Wylie, V.L. Streeter, Fluid transients, McGraw-Hill New York, 1978.

[24] Y. Wang, S. You, H. Zhang, W. Zheng, X. Zheng, Q. Miao, Hydraulic performance optimization of meshed district heating network with multiple heat sources, Energy, 126 (2017) 603-621. https://doi.org/10.1016/j.energy.2017.03.044.

[25] J. Lu, Z. Guan, Numerical Methods for Partial Differential Equations, Tsinghua University Press, Beijing, 2004. [In Chinese].

Highlights:

- DPM and LPM of DH network for hydraulic transient modeling are established.
- Efficient numerical algorithms were presented for the two models.
- Transient time for the flow rate and pressure is analyzed by the two models.
- Flow rate variation of the constant pressure make-up water is simulated by DPM.
- High-frequency hydraulic transient characteristics can be captured by DPM subtly.

Xuejing Zheng, Yaran Wang, Shijun You, Huan Zhang: Conceptualization, Methodology. Boxiao Xu, Yaran Wang: Software, Data curation, Formal analysis, Writing- Original draft preparation. Na wang: Formal analysis. Shen Wei: Writing-Reviewing and Editing.

Declaration of interests

☒The authors declare that they have no known competing financial interests or personal relationships that could have appeared to influence the work reported in this paper.

☐The authors declare the following financial interests/personal relationships which may be considered as potential competing interests: